Structural, Dynamic, and Theoretical Studies of $[Au_nPt_2(PPh_3)_4(\mu\text{-}S)_{2-n}(\mu_3\text{-}S)_nL][PF_6]_n$ [n = 1, L = PPh_3; n = 2, L = $Ph_2PCH_2PPh_2$, $(C_5H_4PPh_2)_2Fe$]

Zhaohui Li, Zhi-Heng Loh, K. F. Mok,* and T. S. Andy Hor*

Department of Chemistry, National University of Singapore, 3 Science Drive 3, Singapore 117543

Received December 9, 1999

Three heterometallic Au−Pt complexes $[Pt_2(PPh_3)_4(\mu\text{-}S)(\mu_3\text{-}S)Au(PPh_3)][PF_6]$ (**2**), $[Pt_2(PPh_3)_4(\mu_3\text{-}S)_2Au_2(\mu\text{-}dppm)][PF_6]_2$ (**3**), and $[Pt_2(PPh_3)_4(\mu_3\text{-}S)_2Au_2(\mu\text{-}dppf)][PF_6]_2$ (**4**) have been synthesized from $Pt_2(PPh_3)_4(\mu\text{-}S)_2$ (**1**) [dppm = $Ph_2PCH_2PPh_2$; dppf = $(C_5H_4PPh_2)_2Fe$] and characterized by single-crystal X-ray crystallography. In **2**, the Au(I) atom is anchored on only one of the sulfur centers. In **3** and **4**, both sulfur atoms are aurated, showing the ability of **1** to support an overhead bridge structure, viz. $[Au_2(P-P)]$, with or without the presence of Au−Au bond. The change of dppf to dppm facilitates such active interactions. Two stereoisomers of complex **3** (**3a,b**) have been obtained and characterized by single-crystal X-ray crystallography. NLDFT calculations on **2** show that the linear coordination mode is stabilized with respect to the trigonal planar mode by 14.0 kJ/mol. All complexes (**2**−**4**) are fluxional in solution with different mechanisms. In **2**, the $[Au(PPh_3)]$ fragment switches rapidly between the two sulfur sites. Our hybrid MM-NLDFT calculations found a transition state in which the Au(I) bears an irregular trigonal planar geometry ($\Delta G^{\ddagger}$ = 19.9 kJ/mol), as well as an intermediate in which Au(I) adopts a regular trigonal planar geometry. Complexes **3a,b** are roughly diastereoisomeric and related by σ (mirror plane) conversion. This symmetry operation can be broken down to two mutually dependent fluxional processes: (i) rapid flipping of the dppm methylene group across the molecular plane defined by the overhead bridge; (ii) rocking motion of the two Au atoms across the S···S axis of the $\{Pt_2S_2\}$ core. Modeling of the former by molecular mechanics yields a steric barrier of 29.0 kJ/mol, close to that obtained from variable-temperature $^{31}P\{^1H\}$ NMR study (33.7 kJ/mol). In **4**, the twisting of the ferrocenyl moiety across the S···S axis is in concert with a rocking motion of the two gold atoms. The movement of dppf is sterically most demanding, and hence, **4** is the only complex that shows a static structure at lower temperatures. Pertinent crystallographic data: (**2**) space group $P\bar{1}$, a = 15.0340(5) Å, b = 15.5009(5) Å, c = 21.9604(7) Å, α = 74.805(1)°, β = 85.733(1)°, γ = 78.553(1)°, R = 0.0500; (**3a**) space group $Pna2_1$, a = 32.0538(4) Å, b = 16.0822(3) Å, c = 18.9388(3) Å, R = 0.0347; (**3b**) space group $Pna2_1$, a = 31.950(2) Å, b = 16.0157(8) Å, c = 18.8460(9) Å, R = 0.0478; (**4**) space group $P2_1/c$, a = 13.8668(2) Å, b = 51.7754(4) Å, c = 15.9660(2) Å, β = 113.786(1)°, R = 0.0649.

Introduction

Although other researchers and we have explored extensively the syntheses of heterometallic sulfide aggregates and clusters using $Pt_2(PPh_3)_4(\mu\text{-}S)_2$ (**1**) as a building block,[1] to date we are still unable to understand some fundamental issues which underpin the coordination behavior of this metalloligand. For example, why does alkylation of **1** with RX give $[Pt_2(PPh_3)_4(\mu\text{-}S)(\mu\text{-}RS)][X]$ but not $[Pt_2(PPh_3)_4(\mu\text{-}RS)_2][X]_2$?[2,3] Why is the Au(I) atom in $[AuPt_2(PPh_3)_5(\mu\text{-}S)_2][X]$ (X = NO_3, BF_4)[4] connected to only one sulfur (and hence linear) ignoring the nearby sulfur (and hence trigonal) when there are ample examples of trigonal Au(I) and cases when **1** serves as a bidentate ligand using both sulfur atoms, e.g. $CoPt_2Cl_2(PPh_3)_4(\mu_3\text{-}S)_2$,[5] $[CuPt_2(PPh_3)_5(\mu_3\text{-}S)_2][X]$ (X = PF_6),[6] etc.? Is the support of a M_2 moiety by $\{Pt_2S_2\}$ dependent on the extent of M−M interaction? The last issue is of particular concern since it is our main target to build heteromultimetallic aggregates from **1**. Unfortunately, almost all examples isolated today are confined to 1:1 addition of a metal fragment with **1** resulting in a $\{MPt_2S_2\}$ core that does not appear to show much interest in further metalation. $[Ag_2\{Pt_2(PPh_3)_4(\mu_3\text{-}S)_2\}_2]^{2+}$ is the only notable exception whereby **1** is in a close-bridging mode supporting an unusual Ag^I-Ag^I bond (Ag−Ag 2.815(4) Å).[7] When we understand the conditions for planting a metal pair on **1**, we will be able to elaborate the aggregation process based on the M_2 rather than $\{Pt_2S_2\}$ core, thus helping to extend the barrier beyond the trimetallic framework. Our recent studies on the $\{Re_2(OR)_2\}$ core demonstrated some significant dynamic behavior of an overhead bridging ligand on this core.[8,9,10] In

* Corresponding authors.

(1) Fong, S. W. A.; Hor, T. S. A. *J. Chem. Soc., Dalton Trans*. **1999**, 639.
(2) Hor, T. S. A. D. Philos. Thesis, University of Oxford, Oxford, U.K., 1983.
(3) Briant, C. E.; Gardnet. C. J.; Hor, T. S. A.; Hewells, N. D.; Mingos, D. M. P. *J. Chem. Soc., Dalton Trans.* **1984**, 2645.
(4) Bos, W.; Bour, J. I.; Schlebos, P. P. J.; Hageman, P.; Bosman, W. P.; Smits, J. M. M.; van Wietmarschen, J. A. C.; Beurskens, P. T. *Inorg. Chim. Acta* **1986**, *119*, 141.
(5) Liu, H.; Tan, A. L.; Mok, K. F.; Hor, T. S. A. *J. Chem. Soc., Dalton Trans*. **1996**, 4023.
(6) Liu, H.; Tan, A. L.; Xu, Y.; Mok, K. F.; Hor, T. S. A. *Polyhedron* **1997**, *16*, 377.
(7) Briant, C. E.; Hor, T. S. A.; Howells, N. D.; Mingos, D. M. P. *J. Organomet. Chem.* **1983**, *256*, C15.
(8) Lam, S.-L.; Cui, Y.-X.; Au-Yeung, S. C. F.; Yan, Y.-K.; Hor, T. S. A. *Inorg. Chem.* **1994**, *33*, 2407.
(9) Low, P. M. N.; Yong, Y. L.; Yan, Y. K.; Hor, T. S. A.; Lam, S.-L.; Chan, K. K.; Wu, C.; Au−Yeung, S. C. F.; Wen, Y.-S.; Liu, L.-K. *Organometallics* **1996**, *15*, 1369.
(10) Jiang, C.; Wen, Y.-S.; Liu, L.-K.; Hor, T. S. A.; Yan, Y. K. *Organometallics* **1998**, *17*, 173.

10.1021/ic991416k CCC: $19.00
Published on Web 10/21/2000

Table 1. Data Collection and Structure Refinement of $[Pt_2(PPh_3)_4(\mu\text{-S})(\mu_3\text{-S})Au(PPh_3)]^+$ (**2**), $[Pt_2(PPh_3)_4(\mu_3\text{-S})_2Au_2(\mu\text{-dppm})]^{2+}$ (**3a**,**b**), and $[Pt_2(PPh_3)_4(\mu_3\text{-S})_2Au_2(\mu\text{-dppf})]^{2+}$ (**4**)

	2	3a	3b	4
chem formula	$C_{90}H_{76}AuF_6O_{0.50}P_6\ Pt_2S_2$	$C_{97}H_{82}Au_2F_{12}P_8Pt_2\ S_2$	$C_{97}H_{82}Au_2F_{12}P_8Pt_2\ S_2$	$C_{106.50}H_{89}Au_2ClF_{12}\ FeP_8Pt_2S_2$
fw	2116.59	2571.62	2571.62	2784.07
l (Å)	0.710 73	0.710 73	0.710 73	0.710 73
T (K)	293(2)	293(2)	293(2)	293(2)
space group	$P\bar{1}$ (No. 2)	$Pna2_1$ (No. 33)	$Pna2_1$ (No. 33)	$P2_1/c$ (No. 14)
a (Å)	15.0340(5)	32.0538(4)	31.950(2)	13.8668(2)
b (Å)	15.5009(5)	16.0822(3)	16.0157(8)	51.7754(4)
c (Å)	21.9604(7)	18.9388(3)	18.8460(9)	15.9660(2)
α (deg)	74.805(1)			
β (deg)	85.733(1)			113.786(1)
γ (deg)	78.553(1)			
V (Å^3)	4839.2(3)	9762.9(3)	9643.6(8)	10489.3(2)
Z	2	4	4	4
r (g/cm^3)	1.453	1.750	1.771	1.763
m (mm^{-1})	4.589	6.094	6.169	5.835
R_1,[a] wR_2[b] ($I > 2\sigma(I)$)	$R_1 = 0.0500$, $wR_2 = 0.1601$	$R_1 = 0.0347$, $wR_2 = 0.0843$	$R_1 = 0.0478$, $wR_2 = 0.1196$	$R_1 = 0.0649$, $wR_2 = 0.1297$
R_1,[a] wR_2[b] (all data)	$R_1 = 0.0718$, $wR_2 = 0.1742$	$R_1 = 0.0493$, $wR_2 = 0.0974$	$R_1 = 0.0763$, $wR_2 = 0.1403$	$R_1 = 0.0859$, $wR_2 = 0.1372$

[a] $R_1 = \Sigma||F_0| - |F_c||/\Sigma|F_0|$. [b] $wR_2 = \{\Sigma w|[(F_0^2 - F_c^2)^2]/\Sigma wF_o^4\}^{1/2}$; $\rho = [(F_0^2,\theta) + 2F_c^2]/3$.

this paper, we shall discuss the assembly of an Au_nPt_2 system that shows different dynamic behaviors with different phosphine ligands on Au(I). We also report an unusual isolation of two stereoisomers that differ only by the orientations of the Au−Au bonds in two rocking positions. Insight into some of the structural and dynamic behaviors has been made possible by a theoretical investigation.

Experimental Section

All solvents were distilled and deoxygenated by argon before use. Complex **1** was synthesized from $PtCl_2(PPh_3)_2$ and $Na_2S\cdot 2H_2O$ according to the literature method.[11] $AuCl(PPh_3)$,[12] $Au_2Cl_2(\mu\text{-dppm})$,[13] and $Au_2Cl_2(\mu\text{-dppf})$[13] were synthesized from $HAuCl_4$. Other chemicals were used as supplied. Elemental analyses were carried out in the Elemental Analysis Laboratory in the Chemistry Department of the National University of Singapore (NUS). Infrared spectra were taken in KBr disk on a Perkin-Elmer 1600 FT-IR spectrophotometer. $^{31}P\{^1H\}$ NMR spectra were taken on a Bruker ACF 300 spectrometer.

Preparations. $[Pt_2(PPh_3)_4(\mu\text{-S})(\mu_3\text{-S})Au(PPh_3)][PF_6]$ (2). A suspension of **1** (0.15 g, 0.1 mmol) and $AuCl(PPh_3)$ (0.049 g, 0.1 mmol) was stirred in MeOH (30 cm^3) for 2 h to give a clear orange solution. The solution was filtered and purified by metathesis with NH_4PF_6 to yield complex **2**. The product was recrystallized in CH_2Cl_2/Et_2O to give orange crystals. Yield: 0.104 g, 49%. Anal. Calcd for $C_{90}H_{76}AuF_6O_{0.50}P_6Pt_2S_2$: C, 51.03; H, 3.59; F, 5.39; P, 8.79; S, 3.02. Found: C, 52.75; H, 3.45; F, 5.68; P, 7.98; S, 2.72. IR (cm^{-1}): 839 vs (PF_6^-). $^{31}P\{^1H\}$ NMR ($CDCl_3$): δ 20.7 ppm (4P, ^1J(P−Pt) 3033 Hz), 31.7 ppm (1P, s).

$[Pt_2(PPh_3)_4(\mu_3\text{-S})_2Au_2(\mu\text{-dppm})][PF_6]_2$ (3a,b). A suspension of **1** (0.15 g, 0.1 mmol) and $Au_2Cl_2(\mu\text{-dppm})$ (0.085 g, 0.1 mmol) was stirred in MeOH (30 cm^3) for 2 h to give a clear pale-yellow solution. The solution was filtered and purified by metathesis with NH_4PF_6 to yield **3**, which was recrystallized in acetone/MeOH (1:3) to give pale-yellow crystals. Yield: 0.145 g, 56%. Anal. Calcd for $C_{97}H_{82}Au_2F_{12}P_8Pt_2S_2$: C, 45.26; H, 3.19; F, 8.87; P, 9.64; S, 2.49. Found: C, 45.73; H, 3.24; F, 8.53; P, 9.24; S, 2.68. IR (cm^{-1}): 839 vs (PF_6^-). $^{31}P\{^1H\}$ NMR (CD_2Cl_2): δ 19.8 ppm (4P, ^1J(P−Pt) 2981 Hz), 31.1 ppm (2P, s).

$[Pt_2(PPh_3)_4(\mu_3\text{-S})_2Au_2(\mu\text{-dppf})][PF_6]_2$ (4). Complex **4** was synthesized in a manner analogous to **3** by using **1** (0.15 g, 0.1 mmol) and $Au_2Cl_2(\mu\text{-dppf})$ (0.103 g, 0.1 mmol) in MeOH (30 cm^3). After 2 h, the resultant clear yellow solution was filtered and purified by metathesis with NH_4PF_6 to yield complex **4**. The product was recrystallized in CH_2Cl_2/MeOH (1:3) mixture to give orange crystals. Yield: 0.135 g, 48.5%. Anal. Calcd for $C_{106.50}H_{89}Au_2ClF_{12}FeP_8Pt_2S_2$: C, 45.91; H, 3.20; F, 8.19; P, 8.91; S, 2.30. Found: C, 45.45; H, 3.45; F, 8.56; P, 8.53; S, 2.53. IR (cm^{-1}): 839 vs (PF_6^-). $^{31}P\{^1H\}$ NMR (CD_2Cl_2): δ 20.9 ppm (4P, b, ^1J(P−Pt) 2991 Hz), 30.0 ppm (2P, b).

X-ray Crystallography. Single crystals of **2** suitable for X-ray diffraction studies were grown from CH_2Cl_2/ether by slow diffusion at room temperature. Single crystals of **3a,b** were grown from acetone/MeOH (1:3) by slow evaporation at room temperature in air while those of **4** were grown from CH_2Cl_2/MeOH (1:3) by slow evaporation at room temperature in air. The crystals were sealed in a quartz capillary with the mother liquor during data collection. Data collection was carried out on a Siemens CCD SMART system. The details of data collection and structure refinement are summarized in Table 1.

The structures of all four complexes were solved by direct methods and remaining non-hydrogen atoms located in difference Fourier maps. Full-matrix least-squares refinements were carried out with anisotropic temperature factors for all non-hydrogen atoms. Hydrogen atoms were placed on calculated positions (C−H 0.96 Å) and assigned isotropic thermal parameters riding on their parent atoms. Initial calculations were carried out on a PC using SHELXTL PC software package; SHELXL-93[14] was used for the final refinement.

Computational Methods. Nonlocal density functional theory (NLDFT) calculations were carried out in GAUSSIAN 98.[15] Gradient corrections were introduced in a self-consistent manner by using the three-parameter hybrid exchange functional of Becke[16] (B3) and the correlation functional of Lee, Yang, and Parr[17] (LYP). Our calculations employ the LanL2DZ basis set, which has been shown to yield qualitatively accurate energies.[18,19,20] This basis set consists of the

(11) Ugo, R.; La Monica, G.; Cenimi, S.; Segre, A.; Conti, F. *J. Chem. Soc. A* **1971**, 522.
(12) Kowala, C.; Swan, J. M. *Aust. J. Chem.* **1966**, *19*, 547.
(13) Hill, T. H.; Girard, G. R.; McCabe, F. L.; Johnson, R. K.; Stupik, P. D.; Zhang, J. H.; Reiff, W. M.; Eggleston, D. S. *Inorg. Chem.* **1989**, *28*, 3529.
(14) Sheldrick, G. M. *SHELXL-93, Program for Crystal Structure Refinement*; University of Göttingen, Göttingen, Germany.
(15) Frisch, M. J.; Trucks, G. W.; Schlegel, H. B.; Scuseria, G. E.; Robb, M. A.; Cheeseman, J. R.; Zakrzewski, V. G.; Montgomery, J. A., Jr.; Stratmann, R. E.; Burant, J. C.; Dapprich, S.; Millam, J. M.; Daniels, A. D.; Kudin, K. N.; Strain, M. C.; Farkas, O.; Tomasi, J.; Barone, V.; Cossi, M.; Cammi, R.; Mennucci, B.; Pomelli, C.; Adamo, C.; Clifford, S.; Ochterski, J.; Petersson, G. A.; Ayala, P. Y.; Cui, Q.; Morokuma, K.; Malick, D. K.; Rabuck, A. D.; Raghavachari, K.; Foresman, J. B.; Cioslowski, J.; Ortiz, J. V.; Baboul, A. G.; Stefanov, B. B.; Liu, G.; Liashenko, A.; Piskorz, P.; Komaromi, I.; Gomperts, R.; Martin, R. L.; Fox, D. J.; Keith, T.; Al-Laham, M. A.; Peng, C. Y.; Nanayakkara, A.; Gonzalez, C.; Challacombe, M.; Gill, P. M. W.; Johnson, B.; Chen, W.; Wong, M. W.; Andres, J. L.; Gonzalez, C.; Head-Gordon, M.; Replogle, E. S.; Pople, J. A. *GAUSSIAN 98, Revision A.7*; Gaussian, Inc.: Pittsburgh, PA, 1998.
(16) Becke, A. D. *J. Chem. Phys.* **1993**, *98*, 5648.
(17) Lee, C.; Yang, W.; Parr, R. G. *Phys. Rev. B* **1988**, *37*, 785.
(18) Bernardi, F.; Bottoni, A.; Calcinari, M.; Rossi, I.; Robb, M. A. *J. Phys. Chem. A* **1997**, *101*, 6310.

Dunning−Huzinaga valence double-ζ basis[21] on H and C and a combination of the quasi-relativistic LanL2 effective core potentials,[22,23,24] and valence double-ζ[23] on P, S, Fe, Pt, and Au. Bond overlap populations were calculated by using Mulliken population analysis. Input structures for single point energy calculations were obtained from X-ray crystallography data. To simplify calculations, the phenyl rings on the phosphines were replaced with H atoms; the P−H bond length was set as the sum of covalent radii of P and H (1.42 Å). Geometry optimizations employ analytic gradients and second derivatives.

Steric effects are expected to be important in the investigation of fluxional behavior. While it has been shown that the replacement of PPh_3 with PH_3 in first-principles calculations allows both electronic structures and bonding interactions to be accurately studied,[25] calculations based on such simplifications do not provide an accurate treatment of steric effects. Hence, to model fluxional behavior accurately, we have employed a hybrid of molecular mechanics (MM) and NLDFT calculations in which the PPh_3 groups were not replaced. MM calculations were carried out with the SYBYL[26] force field implemented in SPARTAN 5.1.[27] The following procedure was used to calculate the steric energy arising from the presence of phenyl rings in our molecules. First, the PH_3 groups in the NLDFT-optimized structures were replaced with PPh_3 groups. Second, a MM optimization of the positions of the phenyl rings was carried out while keeping the positions of the Au, Pt, S, and P atoms frozen. Third, the Au, Pt, and S atoms were replaced with dummy atoms and single point energy calculations were carried out with the same force field. The resultant energies can reasonably be attributed to the steric energies arising from presence of phenyl rings.

MM calculations were also carried out to study the fluxional behavior exhibited by **3**. Calculations were performed on the X-ray crystal structure. Coordinate driving was used to flip the dppm methylene group from one side of the Au_2S_2 plane to the other in 20 steps. Structural parameters for the dppm methylene group and the phenyl substituents on all the phosphines were allowed to vary freely while the positions of the other atoms were frozen.

Results and Discussion

The preparations of complexes **2**−**4** from complex **1** are listed in Scheme 1.

A 1:1 mixture of $AuCl(PPh_3)$ and **1** in MeOH gives rise to $[Pt_2(PPh_3)_4(\mu\text{-}S)(\mu_3\text{-}S)Au(PPh_3)][PF_6]$ (**2**) after metathesis with NH_4PF_6. The $^{31}P\{^1H\}$ NMR spectrum gives a single resonance on the $[Pt_2(PPh_3)_4(\mu\text{-}S)_2]$ moiety, appearing to suggest that $[Au(PPh_3)]$ is symmetrically anchored on the $\{Pt_2S_2\}$ core through the two sulfur atoms. Analysis by X-ray single-crystal diffraction gives a trimetallic complex (Figure 1) isostructural to $[Pt_2(PPh_3)_4(\mu\text{-}S)(\mu_3\text{-}S)Au(PPh_3)][NO_3]$.[4] Selected bond lengths and angles are listed in Table 2. With a near-linear Au(I) geometry (S(1)−Au(3)−P(5) 172.14(8)°), and only one Au−S bond (2.338(2) Å, compared to the nonbonding partner, 3.134(2) Å), it contrasts the trigonal planar geometry found in the Cu(I) and Ag(I) analogues.[6,28] The propensity of Au(I) to adopt a linear coordination mode in its complexes has been attributed to relativistic effects and (to a smaller extent) lanthanide contraction.[29,30] However, ample examples of three-coordinate Au(I)

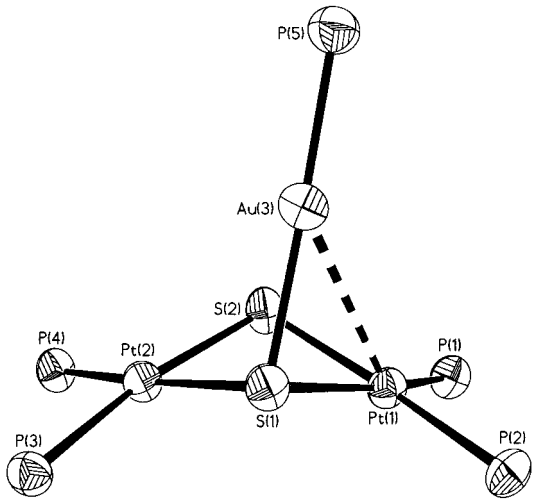

Figure 1. Thermal ellipsoid plot (50% probability) of $[Pt_2(PPh_3)_4(\mu\text{-}S)(\mu_3\text{-}S)Au(PPh_3)]^+$ (**2**) (anion and phenyl rings omitted for clarity).

Scheme 1. Preparations of $[Pt_2(PPh_3)_4(\mu\text{-}S)(\mu_3\text{-}S)Au(PPh_3)]^+$ (**2**), $[Pt_2(PPh_3)_4(\mu_3\text{-}S)_2Au_2(\mu\text{-dppm})]^{2+}$ (**3a,b**), and $[Pt_2(PPh_3)_4(\mu_3\text{-}S)_2Au_2(\mu\text{-dppf})]^{2+}$ (**4**) from $[Pt_2(PPh_3)_4(\mu\text{-}S)_2]$ (**1**)

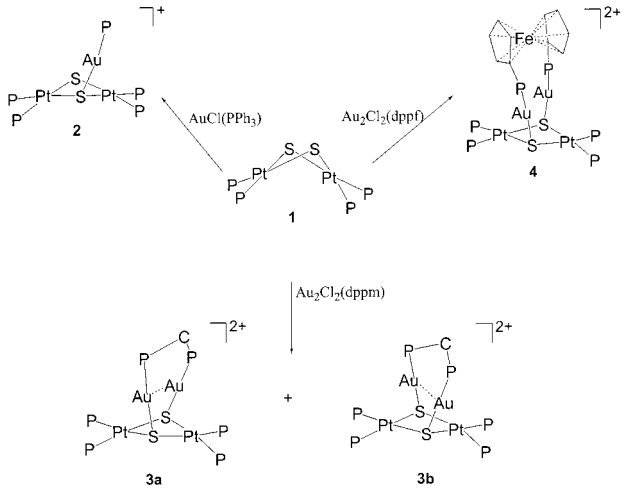

complexes are known,[31,32] e.g. $[NBu_4][Au(dmit)(PPh_3)]$ (dmit = 2-thioxo-1,3-dithiole-4,5-dithiolate),[33] $[\{(Ph_3P)Au\}_4L\}][BF_4]$ (L = propane-1,2,3-trithiolate),[34] $Au_2(\mu\text{-}S_2C_6H_4)(PPh_3)_2$,[35] and $Au_2(MNT)(PMe_3)_2$ (MNT = 1,2-dicyanoethene-1,2-dithiolate-S,S′).[36] The S···S separations in **1** and **2** appear to be ideal for a symmetric disposition of the Au(I) atom between these sulfur atoms. So, why does Au(I) in **2** show such a strong preference for a linear geometry when a trigonal planar one appears to be conducive?

(19) Su, M.-D.; Chu, S.-Y. *Inorg. Chem.* **1998**, *37*, 3400.
(20) Porembski, M.; Weisshaar, J. C. *J. Phys. Chem. A* **2000**, *104*, 1524.
(21) Dunning, T. H., Jr.; Hay, P. J. In *Modern Theoretical Chemistry*; Schaeffer, H. F.; III, Ed.; Plenum: New York, 1976; p 1.
(22) Hay, P. J.; Wadt, W. R. *J. Chem. Phys.* **1985**, 82, 270.
(23) Wadt, W. R.; Hay, P. J. *J. Chem. Phys.* **1985**, *82*, 284.
(24) Wadt, W. R.; Hay, P. J. *J. Chem. Phys.* **1985**, *82*, 299.
(25) Häberlen, O. D.; Rösch, N. *J. Phys. Chem.* **1993**, *97*, 4970.
(26) Clark, M.; Cramer III, R. D.; van Opdensch, N. *J. Comput. Chem.* **1989**, *10*, 982.
(27) SPARTAN 5.1, Wavefunction, Inc., 18401 Von Karman Ave., Ste. 370, Irvine, CA 92612.
(28) Liu, H.; Tan, A. L.; Cheng, C. R.; Mok, K. F.; Hor, T. S. A. *Inorg. Chem.* **1997**, *36*, 2916.
(29) Puddephatt, R. J. In *Comprehensive Coordination Chemistry*; Wilkinson, G., Gillard, R. D., McCleverty, J. A., Eds.; Pergamon: Oxford, U.K., 1987; Vol. 5, p 687.
(30) Puddephatt, R. J. *The Chemistry of Gold*; Elsevier: Amsterdam, 1978; p 15.
(31) Laguna, A. 391.
(32) Fackler, J. P., Jr.; van Zyl, W. E.; Prihoda, B. A. *Gold: Progress in Chemistry, Biochemistry and Technology*; Schmidbaur, H., Ed.; Wiley: Chichester, U.K., 1999; p 805.
(33) Cerrada, E.; Jones, P. G.; Laguna, A.; Laguna, M. *Inorg. Chem.* **1996**, *35*, 2995.
(34) Sladek, A.; Schmidbaur, H. *Inorg. Chem.* **1996**, *35*, 3268.
(35) Dávila, R. M.; Elduque, A.; Grant, T.; Staples, R. J.; Fackler, J. P., Jr. *Inorg. Chem.* **1993**, *32*, 1749.
(36) Dávila, R. M.; Staples, R. J.; Elduque, A.; Harlass, M. M.; Kyle, L.; Fackler, J. P., Jr. *Inorg. Chem.* **1994**, *33*, 5940.

Table 2. Selected Bond Lengths (Å) and Bond Angles (deg) of $[Pt_2(PPh_3)_4(\mu\text{-}S)(\mu_3\text{-}S)Au(PPh_3)]^+$ (**2**), $[Pt_2(PPh_3)_4(\mu_3\text{-}S)_2Au_2(\mu\text{-}dppm)]^{2+}$ (**3a**,**b**), and $[Pt_2(PPh_3)_4(\mu_3\text{-}S)_2Au_2(\mu\text{-}dppf)]^{2+}$ (**4**)

(1) $[Pt_2(PPh_3)_4(\mu\text{-}S)(\mu_3\text{-}S)Au(PPh_3)][PF_6]$ (**2**)			
Pt(1)−P(1)	2.290(2)	Pt(1)−P(2)	2.303(2)
Pt(1)−S(2)	2.356(2)	Pt(1)−S(1)	2.379(2)
Pt(1)−Au(3)	3.103(1)	Pt(2)−P(4)	2.289(2)
Pt(2)−P(3)	2.315(2)	Pt(2)−S(2)	2.337(2)
Pt(2)−S(1)	2.360(2)	Au(3)−P(5)	2.252(2)
Au(3)−S(1)	2.338(2)	Au(3)···Pt(2)	3.495(5)
Au(3)···S(2)	3.134(2)	Pt(1)···Pt(2)	3.390(5)
S(1)···S(2)	3.075(3)		
Dihedral Angle Pt(1)S(1)S(2)Pt(2): 140.8°			
P(1)−Pt(1)−P(2)	105.86(9)	P(1)−Pt(1)−S(2)	83.71(8)
P(2)−Pt(1)−S(2)	170.41(8)	P(1)−Pt(1)−S(1)	164.33(8)
P(2)−Pt(1)−S(1)	89.46(8)	S(2)−Pt(1)−S(1)	81.01(7)
P(1)−Pt(1)−Au(3)	127.79(6)	P(2)−Pt(1)−Au(3)	104.31(7)
S(2)−Pt(1)−Au(3)	68.51(6)	S(1)−Pt(1)−Au(3)	48.29(5)
P(4)−Pt(2)−P(3)	100.57(8)	P(4)−Pt(2)−S(2)	90.64(8)
P(3)−Pt(2)−S(2)	168.29(8)	P(4)−Pt(2)−S(1)	172.39(8)
P(3)−Pt(2)−S(1)	86.90(7)	S(2)−Pt(2)−S(1)	81.82(7)
P(5)−Au(3)−S(1)	172.14(8)	P(5)−Au(3)−Pt(1)	136.83(7)
P(5)−Au(3)−Pt(1)	136.83(7)	S(1)−Au(3)−Pt(1)	49.45(6)
Au(3)−S(1)−Pt(2)	96.17(7)	Au(3)−S(1)−Pt(1)	82.26(6)
Pt(2)−S(1)−Pt(1)	91.36(7)	Pt(2)−S(2)−Pt(1)	92.52(7)
(2) $[Pt_2(PPh_3)_4(\mu_3\text{-}S)_2Au_2(\mu\text{-}dppm)][PF_6]_2$ (**3a**)			
Pt(1)−P(2)	2.303(2)	Pt(1)−P(1)	2.308(2)
Pt(1)−S(2)	2.371(2)	Pt(1)−S(1)	2.392(2)
Pt(2)−P(4)	2.300(2)	Pt(2)−P(3)	2.302(2)
Pt(2)−S(1)	2.359(2)	Pt(2)−S(2)	2.390(2)
Au(3)−P(5)	2.278(2)	Au(3)−S(1)	2.318(2)
Au(3)−S(2)	3.777(2)	Pt(1)···Pt(2)	3.387(4)
Au(3)···Au(4)	2.916(1)	Au(4)−P(6)	2.282(2)
Au(4)−S(2)	2.332(2)	Pt(1)···Au(4)	3.251(1)
Au(4)−S(1)	3.752(2)	S(1)···S(2)	3.178(5)
Au(4)···Pt(2)	3.840(2)	Au(3)···Pt(1)	3.738(4)
Au(3)···Pt(2)	3.395(2)	P(5)−C(85)	1.857(8)
P(6)−C(85)	1.836(9)		
Dihedral Angle Pt(1)S(1)S(2)Pt(2): 141.4°			
P(2)−Pt(1)−P(1)	101.54(8)	P(2)−Pt(1)−S(2)	168.05(8)
P(1)−Pt(1)−S(2)	90.06(8)	P(2)−Pt(1)−S(1)	84.40(7)
P(1)−Pt(1)−S(1)	170.52(8	S(2)−Pt(1)−S(1)	83.72(6)
P(2)−Pt(1)−Au(4)	133.28(6)	P(1)−Pt(1)−Au(4)	98.96(6)
S(2)−Pt(1)−Au(4)	45.78(5)	S(1)−Pt(1)−Au(4)	81.82(5)
P(4)−Pt(2)−P(3)	99.23(8)	P(4)−Pt(2)−S(1)	168.71(7)
P(3)−Pt(2)−S(1)	90.89(7)	P(4)−Pt(2)−S(2)	85.75(7)
P(3)−Pt(2)−S(2)	174.77(7)	S(1)−Pt(2)−S(2)	84.01(7)
P(5)−Au(3)−S(1)	174.88(8)	P(5)−Au(3)−Au(4)	88.15(6)
S(1)−Au(3)−Au(4)	90.84(5)	P(6)−Au(4)−S(2)	175.54(7)
P(6)−Au(4)−Au(3)	91.64(7)	S(2)−Au(4)−Au(3)	91.36(5)
P(6)−Au(4)−Pt(1)	131.24(7)	S(2)−Au(4)−Pt(1)	46.77(5)
Au(3)−Au(4)−Pt(1)	74.41(12)	Au(3)−S(1)−Pt(2)	93.08(7)
Au(3)−S(1)−Pt(1)	105.08(8)	Pt(2)−S(1)−Pt(1)	90.96(7)
Au(4)−S(2)−Pt(1)	87.45(7)	Au(4)−S(2)−Pt(2)	108.80(8)
Pt(1)−S(2)−Pt(2)	90.71(7)		
(3) $[Pt_2(PPh_3)_4(\mu_3\text{-}S)_2Au_2(\mu\text{-}dppm)][PF_6]_2$ (**3b**)			
Pt(1)−P(2)	2.320(4)	Pt(1)−P(1)	2.270(3)
Pt(1)−S(2)	2.365(3)	Pt(1)−S(1)	2.379(3)
Pt(2)−P(4)	2.271(3)	Pt(2)−P(3)	2.316(3)
Pt(2)−S(1)	2.396(3)	Pt(2)−S(2)	2.331(3)
Au(3)−P(5)	2.265(3)	Au(3)−S(1)	2.335(3)
Au(3)−S(2)	3.723(6)	Pt(1)···Pt(2)	3.373(5)
Au(3)···Au(4)	2.905(6)	Au(4)−P(6)	2.258(3)
Au(4)−S(2)	2.307(3)	Pt(1)···Au(3)	3.235(7)
Au(4)−S(1)	3.786(5)	S(1)···S(2)	3.170(7)
Au(4)···Pt(2)	3.376(7)	Au(3)···Pt(2)	3.823(6)
P(5)−C(85)	1.802(14)	P(6)−C(85)	1.858(13)
Dihedral Angle Pt(1)S(1)S(2)Pt(2): 141.6°			
P(2)−Pt(1)−P(1)	101.54(13)	P(2)−Pt(1)−S(2)	169.81(2)
P(1)−Pt(1)−S(2)	85.37(12)	P(2)−Pt(1)−S(1)	89.91(12)
P(1)−Pt(1)−S(1)	169.08(12)	S(2)−Pt(1)−S(1)	83.86(10)
P(2)−Pt(1)−Au(3)	98.40(10)	P(1)−Pt(1)−Au(3)	133.66(9)
S(2)−Pt(1)−Au(3)	81.73(7)	S(1)−Pt(1)−Au(3)	46.09(8)
P(4)−Pt(2)−P(3)	99.10(13)	P(4)−Pt(2)−S(2)	91.75(11)
P(3)−Pt(2)−S(2)	167.96(11)	P(4)−Pt(2)−S(1)	175.65(11)
P(3)−Pt(2)−S(2)	167.96(11)	S(1)−Pt(1)−S(2)	83.86(10)
P(5)−Au(3)−S(1)	174.82(12)	P(5)−Au(3)−Au(4)	92.43(11)
S(1)−Au(3)−Au(4)	91.86(8)	P(6)−Au(4)−S(2)	175.05(7)
P(6)−Au(4)−Au(3)	87.46(10)	S(2)−Au(4)−Au(3)	90.40(8)
P(5)−Au(3)−Pt(1)	131.64(10)	S(1)−Au(3)−Pt(1)	47.22(7)
Au(4)−Au(3)−Pt(1)	74.28(2)	Au(3)−S(1)−Pt(2)	107.84(12)
Au(3)−S(1)−Pt(1)	86.69(10)	Pt(2)−S(1)−Pt(1)	89.90(10)
Au(3)−S(1)−Pt(1)	86.69(10)	Au(3)−S(1)−Pt(2)	107.84(12)
Pt(1)−S(1)−Pt(2)	89.90(10)		
(4) $[Pt_2(PPh_3)_4(\mu_3\text{-}S)_2Au_2(\mu\text{-}dppf)][PF_6]_2$ (**4**)			
Pt(1)−P(2)	2.283(3)	Pt(1)−P(1)	2.301(2)
Pt(1)−S(1)	2.349(2)	Pt(1)−S(2)	2.368(3)
Pt(2)−P(4)	2.294(3)	Pt(2)−P(3)	2.301(3)
Pt(2)−S(2)	2.351(2)	Pt(2)−S(1)	2.375(2)
Au(3)−P(5)	2.265(3)	Au(3)−S(1)	2.294(2)
Au(3)−S(2)	4.263(2)	Au(4)−S(1)	3.964(3)
Au(4)−P(6)	2.267(3)	Au(4)−S(2)	2.296(3)
Au(3)−Au(4)	3.759(3)	Au(3)−Pt(1)	3.707(4)
Au(3)−Pt(2)	3.966(3)	Au(4)−Pt(1)	3.760(5)
Pt(1)···Pt(2)	3.378(5)	S(1)···S(2)	3.128(3)
Au(4)−Pt(2)	3.605(2)		
Dihedral Angle Pt(1)S(1)S(2)Pt(2): 140.5°			
P(2)−Pt(1)−P(1)	99.09(10)	P(2)−Pt(1)−S(1)	93.18(9)
P(1)−Pt(1)−S(1)	166.77(9)	P(2)−Pt(1)−S(2)	174.97(9)
P(1)−Pt(1)−S(2)	84.38(9)	S(1)−Pt(1)−S(2)	83.08(8)
P(4)−Pt(2)−P(3)	98.76(10)	P(4)−Pt(2)−S(2)	91.77(9)
P(3)−Pt(2)−S(2)	169.43(9)	P(4)−Pt(2)−S(1)	171.13(9)
P(3)−Pt(2)−S(1)	86.56(9)	S(2)−Pt(2)−S(1)	82.88(8)
P(5)−Au(3)−S(1)	168.41(10)	P(6)−Au(4)−S(2)	164.64(11)
Au(3)−S(1)−Pt(1)	105.94(10)	Au(3)−S(1)−Pt(2)	116.30(11)
Pt(1)−S(1)−Pt(2)	91.31(8)	Au(4)−S(2)−Pt(2)	101.70(9)
Au(4)−S(2)−Pt(1)	107.42(10)	Pt(2)−S(2)−Pt(1)	91.44(9)

First-principle NLDFT calculations were performed on $[Pt_2(PH_3)_4(\mu\text{-}S)(\mu_3\text{-}S)Au(PH_3)]^+$ (**2a**) to gain insight into the above question. Our calculations show that the linear coordination mode is preferred over the trigonal mode by 14.0 kJ/mol. Structures of linear and trigonal forms of complex **2a** obtained from NLDFT geometry optimization are shown in Figure 2; their bond parameters are summarized in Table 3. To verify the accuracy of the geometry optimization results, we performed a similar series of calculations on the Ag(I) analogue of **2a**. In agreement with the reported X-ray crystal structure,[28] our calculations on the Ag(I) analogue reveal a preference for the trigonal planar mode. Although the sulfur atoms in metalloligand **1** are known to be electron-rich, the binding of a $[Au(PPh_3)]^+$ cation onto the neutral metalloligand causes the complex to gain an overall positive charge. The resultant decrease in the Mulliken charge of the μ_2-sulfur (from −0.130 e in $Pt_2(PH_3)_4(\mu\text{-}S)_2$ to −0.040 in **2a**) decreases its ability to bind the Au(I) fragment to form a trigonal planar Au(I) geometry. Such an effect is evident from the smaller Au−S bond overlap population in trigonal mode (0.253, 0.253 e) compared to that of the single Au−S bond in the linear mode (0.482 e). We note that the bulk of the literature trigonal planar Au(I) complexes involves dithiolate ligands.[31,32] This is hardly surprising since the strong σ-donating nature of the sulfur atoms in these dianionic ligands enables them to coordinate to the Au(I) in a bidentate fashion.

Similar reaction of **1** with $Au_2Cl_2(\mu\text{-dppm})$ in MeOH gives rise to $[Pt_2(PPh_3)_4(\mu_3\text{-}S)_2Au_2(\mu\text{-dppm})][PF_6]_2$ (**3**) after metathesis with NH_4PF_6. Two stereoisomers of complex **3** (**3a,b**) were obtained and characterized by X-ray crystallography. Figure 3 is the structure of one of the stereoisomer, **3a**. The X-ray crystallography shows a $\{Pt_2S_2\}$ ring structure with the $Au_2(\mu\text{-dppm})$ moiety serving as an over-head bridge across the sulfur sites. With short Au···Au distances (2.916(1) Å in **3a** and 2.905(6) Å in **3b**), one may view these as "face-to-face" Au_2 structures supported by two bridging ligands (dppm and **1**) on either side of the Au−Au bond. These distances suggest a

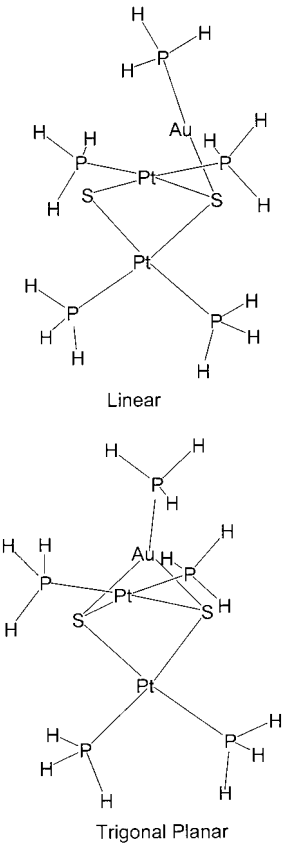

Figure 2. Linear and trigonal planar structures of $[Pt_2(PH_3)_4(\mu\text{-}S)(\mu_3\text{-}S)Au(PH_3)]^+$ (**2a**) obtained from NLDFT geometry optimization.

Table 3. Selected Bond Lengths (Å) and Bond Angles (deg) of Linear and Trigonal Planar Forms of $[Pt_2(PH_3)_4(\mu\text{-}S)(\mu_3\text{-}S)Au(PH_3)]^+$ (**2a**) Obtained from NLDFT Geometry Optimization

	linear coord	trigonal planar coord
Au(3)−P(5)	2.41	2.41
Au(3)−S(1)	2.44	2.70
Pt(1)−S(1)	2.46	2.45
Pt(1)−S(2)	2.43	2.45
Pt(1)−P(1)	2.38	2.39
Pt(1)−P(2)	2.41	2.39
P(5)−Au(3)−S(1)	176.6	143.3
Au(3)−S(1)−Pt(1)	93.8	83.9
S(1)−Pt(1)−S(2)	83.6	82.2
P(1)−Pt(1)−P(2)	99.3	98.3
Pt(1)−S(1)−S(2)−Pt(2)	133.5	126.0

considerable aurophilic interaction and are comparable to those in metallic gold (2.884 Å), Au_2(MNT)[P(OPh)$_3$] (MNT = 1,2-dicyanoethene-1,2-dithiolate-S,S′) (2.991(1) Å),[36] and $Au_2(\mu$-dmpm)(*i*-MNT) (dmpm = bis(dimethylphosphino)methane) (2.925(3) Å).[37] Complex **3** is hence an unusual example that illustrates that both sulfur atoms of **1** can be engaged to sustain a M−M bond, which is reinforced by the opposite dppm ligand.

Replacement of dppm by dppf in the above synthesis results in $[Pt_2(PPh_3)_4(\mu_3\text{-}S)_2Au_2(\mu\text{-dppf})][PF_6]_2$ (**4**) (Figure 4). The Au···Au distance increases significantly to 3.759(3) Å, which is considerably larger than the sub-van der Waals distances in intermolecular Au−Au complexes (ca. 3.05 Å)[38] and must be treated as nonbonding. Although dppf has a larger bite angle than dppm,[39] there are ample examples of closer Au···Au

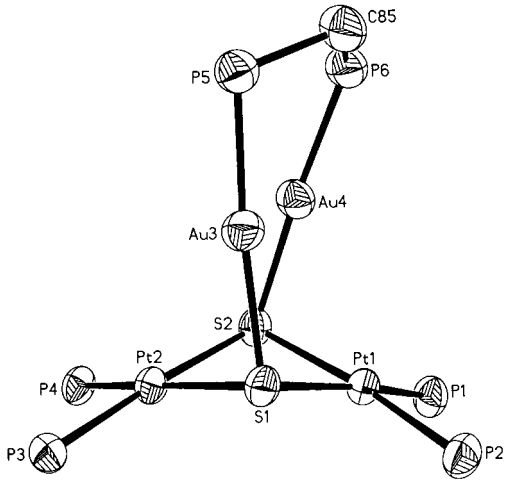

Figure 3. Thermal ellipsoid plot (50% probability) of $[Pt_2(PPh_3)_4(\mu_3\text{-}S)_2Au_2(\mu\text{-dppm})]^{2+}$ (**3a**) (phenyl rings omitted for clarity).

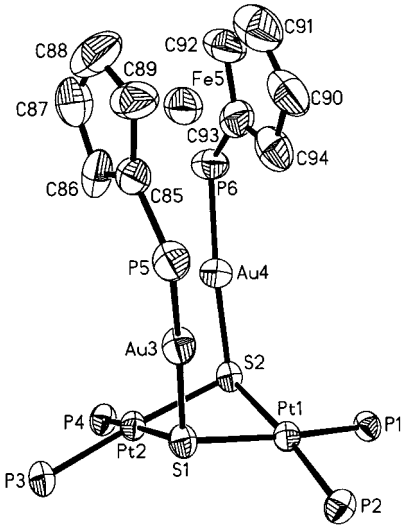

Figure 4. Thermal ellipsoid plot (50% probability) of $[Pt_2(PPh_3)_4(\mu_3\text{-}S)_2Au_2(\mu\text{-dppf})]^{2+}$ (**4**) (phenyl rings omitted for clarity).

interactions sustainable by dppf, e.g. $Au_2(\mu$-S)(μ-dppf) (2.8820(10) Å),[40] [(μ-Au_2dppf){S(Au_2dppf)}$_2$](CF$_3$SO$_3$)$_2$ (2.920-(2), 2.905(2), 2.922(2) Å),[40] [{S(Au_2dppf)}$_2${Au(C$_6$F$_5$)$_2$}][CF$_3$-SO$_3$] (2.9511(9), 2.9158(9) Å),[41] and S(Au_2dppf)[Au(C$_6$F$_5$)$_3$]$_2$ (2.9561(7) Å).[42] The exact reasons for the nonbonding Au···Au interaction in **4** remain unclear. Nevertheless, these results conclude that, for a M_2 unit to anchor on **1**, the latter does not necessarily impose M···M interaction; this inherent flexibility of **1** makes it uniquely suitable for a range of aggregate and cluster expansion reactions. The sharp contrast in the Au···Au distances in **3** and **4** (2.916(1) and 3.759(3) Å, respectively) is not translated to any significant differences in the S···S distances (3.178(5) and 3.128(3) Å, respectively) or the Pt−S−S−Pt dihedral angles (141.4 and 140.5°, respectively). This again reflects the adaptive nature of the ligand.[1]

The $^{31}P\{^1H\}$ NMR spectrum of **2** in $CDCl_3$ suggests that all the phosphines on the two Pt centers are equivalent. This clearly

(37) Tang, S. S.; Chang, C.-P.; Lin, I. J. B.; Liou, L.-S.; Wang, J.-C. *Inorg. Chem*. **1997**, *36*, 2294.
(38) Schmidbaur, H. *Chem. Soc. Rev*. **1995**, 391.
(39) Dierkes, P.; van Leeuwen, P. W. N. M. *J. Chem. Soc., Dalton Trans*. **1999**, 1519.
(40) Canales, F.; Cimeno, M. C.; Laguna, A.; Jones, P. G. *J. Am. Chem. Soc*. **1996**, *118*, 4839.
(41) Calhorda, M. J.; Canales, F.; Gimeno, M. C.; Jiménez, J.; Jones, P. G.; Laguna, A.; Veiros, L. F. *Organometallics* **1997**, *16*, 3837.
(42) Canales, F.; Gimeno, M. C.; Laguna, A.; Jones, P. G. *Organometallics* **1996**, *15*, 3412.

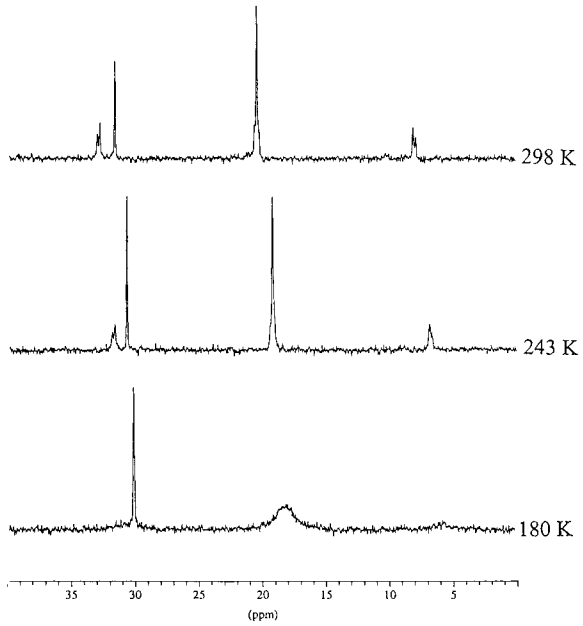

Figure 5. Variable-temperature $^{31}P\{^1H\}$ NMR of $[Pt_2(PPh_3)_4(\mu\text{-}S)(\mu_3\text{-}S)Au(PPh_3)]^+$ (**2**) in CD_2Cl_2.

Scheme 2. Mechanistic Model Used in the Theoretical Calculation of $[Pt_2(PPh_3)_4(\mu\text{-}S)(\mu_3\text{-}S)Au(PPh_3)][PF_6]$ (**2**) Showing Rapid Flipping of the $[Au(PPh_3)]$ between Two Sulfur Atoms

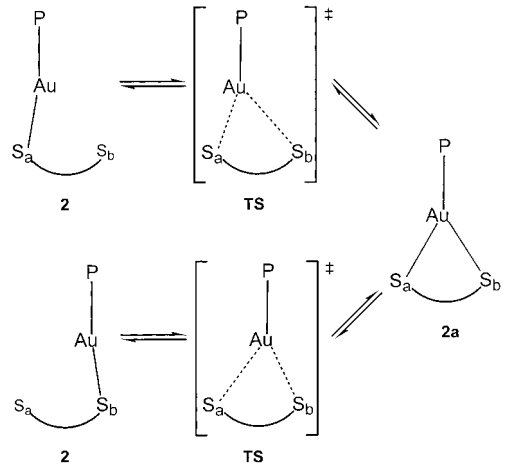

violates the asymmetric disposition of the $[Au(PPh_3)]$ moiety as found in the crystal structure. Variable-temperature $^{31}P\{^1H\}$ NMR analysis reveals that peak broadening begins at 193 K. However, the inequivalent phosphines remain indiscernible even at the lower limit of 180 K (Figure 5). These suggest that **2** is fluxional in the NMR time-scale involving probably a rapid flipping of the $[Au(PPh_3)]$ moiety between the two sulfur centers, perhaps going through a trigonal planar state as in its M(I) analogues (M = Cu, Ag)[6,28] (Scheme 2). A related fluxional process was reported in AuCl(ttp) (ttp = trithiapentalene) whereby the Au center migrates among the three S atoms of the trithiapentalene.[43] We decided to gain more insight into such fluxional process by a theoretical study. NLDFT calculations reveal the presence of a transition state in which the Au(I) bears an irregular trigonal planar geometry. The imaginary frequency of the unstable normal mode is -21.2 cm^{-1}. Comparison of the Au−S distances found in the TS (2.460 and 3.259 Å) to those found in the optimized geometry of **2** (2.443 and 3.379 Å) shows an inclination of the $[Au(PH_3)]$ fragment toward the neighboring sulfur atom in the transition state. Mulliken population analysis yields Au−S overlap populations of 0.468 and 0.012 e; the overlap populations for the corresponding bonds in the optimized geometry of **2** are 0.482 and −0.012 e. The highest occupied molecular orbital (HOMO) resides primarily on the μ_2-sulfur atom, and a weak antibonding interaction along the dissociating Au−S bond is evident. These results suggest a fluxional process involving Au−S bond cleavage and almost concomitant formation of another. At the NLDFT level of theory, the $\Delta G^{\ddagger}$ value calculated for this fluxional process is 8.2 kJ/mol. Hybrid MM-NLDFT calculations yield an overall $\Delta G^{\ddagger}$value of 19.9 kJ/mol; such a small value explains our inability to obtain a resolved $^{31}P\{^1H\}$ NMR spectrum even at 180 K. The close proximity of the two sulfur atoms ensures that such interconversion is rapid on the NMR time scale. By using NLDFT geometry optimization, we also found an intermediate in which the Au(I) bears a regular trigonal planar geometry. Surprisingly, our calculations predict that the intermediate is located 5.8 kJ/mol above the TS. However, applying our hybrid MM-NLDFT method results in a lowering of the energy of the intermediate to 18.9 kJ/mol below the TS. The short nonbonding Au···Pt contact (3.103(1) Å) is not an indication of direct M−M bonds,[44] and the Pt(II) centers are unlikely to be involved in this fluxional process.

Similar to **2**, the single resonance (δ 19.8 ppm) observed for the phosphines on the Pt in the room-temperature $^{31}P\{^1H\}$ NMR spectrum of **3** is also in disagreement with the solid-state structure. With the central methylene group on the dppm residing on either side of the $\{Au_2S_2\}$ plane, the two PtP_2 moieties should be chemically inequivalent. Rapid flipping of the methylene must contribute to the equivalence of all the phosphines on platinum. A similar phenomenon has been observed in $Re_2(\mu\text{-}OMe)_2(\mu\text{-dppm})(CO)_6$.[9] Indeed, at low temperatures, the fluxional motion slows down and the signal broadens. At 193 K, two broad peaks begin to emerge at δ 22.8 and 15.7 ppm (Figure 6). The $\Delta G^{\ddagger}$ value of 33.7 kJ/mol calculated from the coalesce temperature is close to the energy barrier to that reported in $Cu_2Ru_4(\mu_3\text{-}H)_2(\mu\text{-dppe})(CO)_{12}$ (37 ± 1 kJ/mol)[45] and is in agreement with the magnitude of the steric barrier obtained from MM calculations (29.0 kJ/mol). There exists another fluxional process involving the rocking motion of the Au_2 unit, which can also make the phosphines equivalent (Scheme 3). Fortuitously we have isolated two types of crystals in a chemically pure crystalline sample of **3**. X-ray structural analysis of these crystals revealed two stereoisomers (**3a,b**), which are roughly mirror images, related by the Au rocking motion (Figure 7). In this motion, the Au−Au bond swings back and forth across the S···S axis. A related rocking motion has been proposed in $Au_2Ru_4(BH)(\mu\text{-dppf})(CO)_{12}$,[46] but this is the first isolation and structural verification of such stereoisomers related by fluxionality.

Complex **4** behaves similarly by showing only one set of phosphines on the Pt (δ 20.9 ppm) at room temperature, except that the peak is the broadest among all the present complexes.

(43) Wang, S.; Fackler, J. P. *J. Chem. Soc., Chem. Commun.* **1988**, 22.

(44) Our NLDFT calculations revealed a negative overlap population along the Pt−Au bond, confirming the absence of any bonding interaction between the two metal centers. The disposition of the $[Au(PPh_3)]$ fragment toward one of the Pt centers is likely a result of crystal packing forces instead of active Pt−Au bonding interaction.

(45) Salter, L. D.; Sik, V.; Williams, S. A.; Adatia, T. *J. Chem. Soc., Dalton Trans*. **1996**, 643.

(46) Draper, S. M.; Housecroft, C. E.; Rheingold, A. L. *J. Organomet. Chem.* **1992**, *435*, 9.

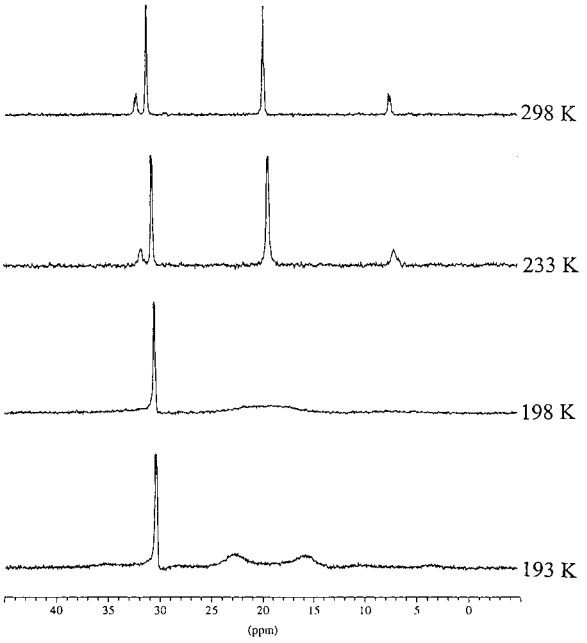

Figure 6. Variable-temperature $^{31}P\{^1H\}$ NMR of $[Pt_2(PPh_3)_4(\mu_3\text{-}S)_2Au_2(\mu\text{-dppm})]^{2+}$ (**3**) in CD_2Cl_2.

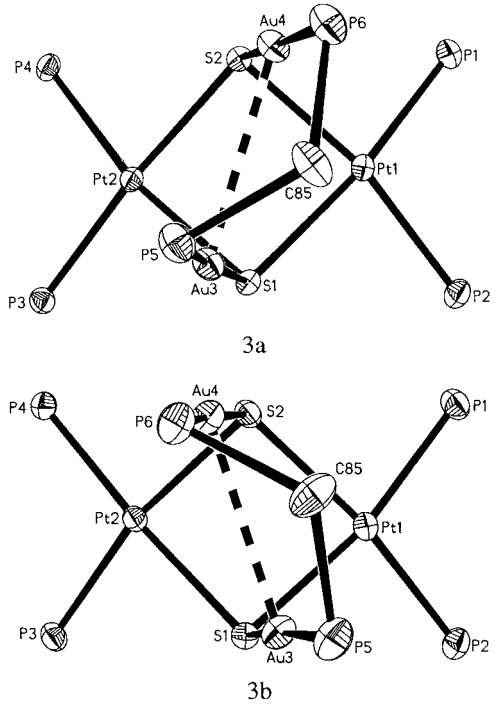

Figure 7. Two stereoisomers of $[Pt_2(PPh_3)_4(\mu_3\text{-}S)_2Au_2(\mu\text{-dppm})]^{2+}$ (**3a,b**).

Accordingly the coalescence temperature (T_c) registered at 233 K is also the highest in this series; at ≤233 K, two distinct peaks (16.3 and 25.8 ppm) are clearly discernible (Figure 8). The $\Delta G^{\ddagger}$ value (47.1 kJ/mol) is similar to that reported for $Re_2(\mu\text{-OMe})_2(\mu\text{-dppf})(CO)_6$ (46.4 ± 0.1 kJ/mol).[8] These results, together with those from our studies of $Re_2(\mu\text{-OR})_2(\mu\text{-dppf})(CO)_6$ (R = H, Me, Et and Ph),[8,10] are consistent with two mutually dependent fluxional processes: (i) the twisting motion of the dppf ligand with respect to the S−S axis; (ii) the rocking motion of the Au_2 moiety (Scheme 3).

All three complexes (**2**−**4**) undergo different fluxional mechanisms, but only **4** shows a static structure at lower temperature limit of time scale. This is attributed to the steric

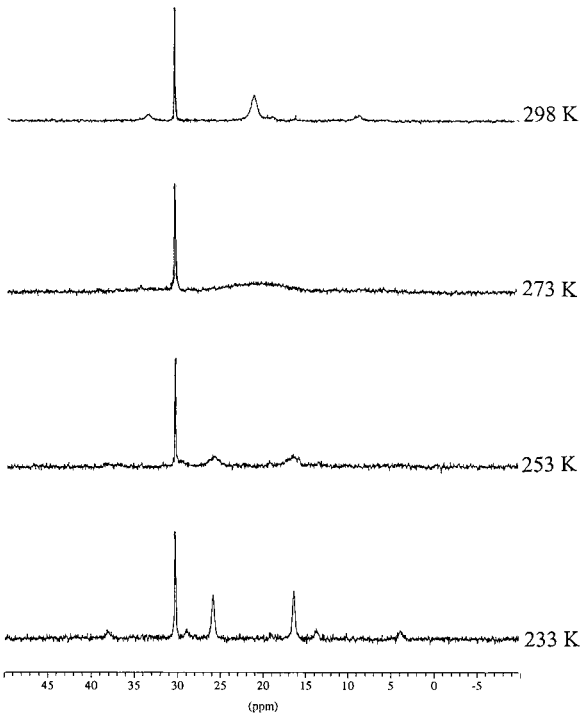

Figure 8. Variable-temperature $^{31}P\{^1H\}$ NMR of $[Pt_2(PPh_3)_4(\mu_3\text{-}S)_2Au_2(\mu\text{-dppf})]^{2+}$ (**4**) in CD_2Cl_2.

Scheme 3. Rocking Motion of the Two Au Atoms across the S···S axis and the Rapid Flipping of the dppm Methylene Group

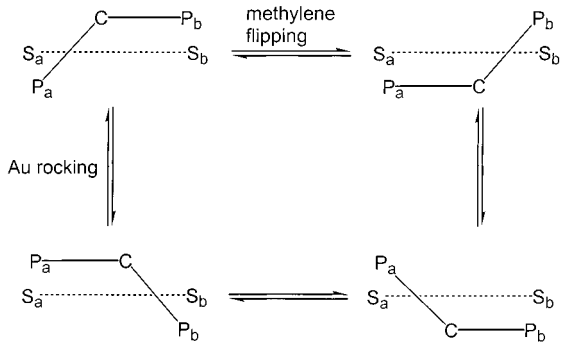

demand associated with the migratory motion of a large ligand like dppf. This study demonstrated that, in conjunction with X-ray crystallography and variable-temperature NMR, computational calculations using NLDFT and MM allowed us to gain a better understanding of the structural and dynamic behaviors and their relationship. This helps us to realize our long-term objective in designing heteromultimetallic architecture with better control of the molecular behavior.

Acknowledgment. The authors acknowledge the National University of Singapore (NUS) (Grant RP 960673) for financial support. Z.L. thanks NUS for a research scholarship award. Technical support from the Department of Chemistry of NUS is appreciated.

Supporting Information Available: Tables of Cartesian coordinates and X-ray crystallographic files in CIF format for the structure determinations of $[Pt_2(PPh_3)_4(\mu\text{-}S)(\mu_3\text{-}S)Au(PPh_3)][PF_6]$, $[Pt_2(PPh_3)_4(\mu_3\text{-}S)_2Au_2(\mu\text{-dppm})][PF_6]_2$, and $[Pt_2(PPh_3)_4(\mu_3\text{-}S)_2Au_2(\mu\text{-dppf})][PF_6]_2$ [dppm = $Ph_2PCH_2PPh_2$; dppf = $(C_5H_4PPh_2)_2Fe$]. The material is available free of charge via the Internet at http://pubs.acs.org.

IC991416K